ENGINEERING RESEARCH JOURNAL (ERJ)
Vol. 1, No. 42 October 2019, pp. 37-44.
Journal Homepage: www.feng.bu.edu.eg

CFD Investigation of the Performance of a Conventional Semi-circular Two Bladed SSWT

Medhat E. M. Abu Khers[1], Mahmoud Fouad[2], Taher Halawa[2]

[1]PhD Student, [2]Professor, [3]Associate Professor
Mechanical Power Engineering Department,
Faculty of Engineering, Cairo University, Giza, Egypt

Abstract. The purpose of this study is to make a numerical simulation of the previously reported experimental results dealing with the performance of the conventional semi-circular two bladed SSWT based on the relationships between torque coefficients and different tip speed ratios λ, to be in comparison with the CFD results. The present investigation demonstrates absolute error growth of order ~ 0.01 within specified range of λ between CFD and the available experimental data.

Keywords: CFD, Savonius style wind turbine; Power coefficient; Torque coefficient; Tip speed ratio.

Nomenclature

ρ	density of air (kg/m^3)
ω	rotational speed of the turbine (rad/s)
Θ	turbine angle to the wind direction (°)
A	swept area of the turbine (m2)
C_P	power coefficient
C_T	torque coefficient
d	chord length of the blades (m)
D	outer diameter of the turbine (m)
V	free stream wind speed (m/s)
D_O	end plate diameter (m)
H	height of the turbine (m)
$P_{available}$	power available in the wind (W)
$P_{turbine}$	power produced by the turbine
R	radius of rotation of the turbine
R_e	Reynolds number
SSWT	Savonius-style wind turbine
T	dynamic torque on the turbine
T_S	static torque on the turbine
TSR	tip speed ratio

1. INTRODUCTION

Energy represents one of the most human basic needs for life along with water, food, and air. It is vital for all life necessities in general, such as lighting, air conditioning, cooling and heating. Most of this energy comes from fossil fuels formed by buried plants in the depths of the earth over millions of years leading to depositing of coal, oil and natural gas, which represent non-renewable sources. However, the exact reserve of these energy sources is limited, as they need millions of years to be reproduced. It was established that coal reserves will be available up to 2112, and they will be the only fossil fuel source remaining after 2042 [1]. That result was in accordance with the Hubbert assumption who assigned his famous curve "Fig. 1" in 1956 [2].

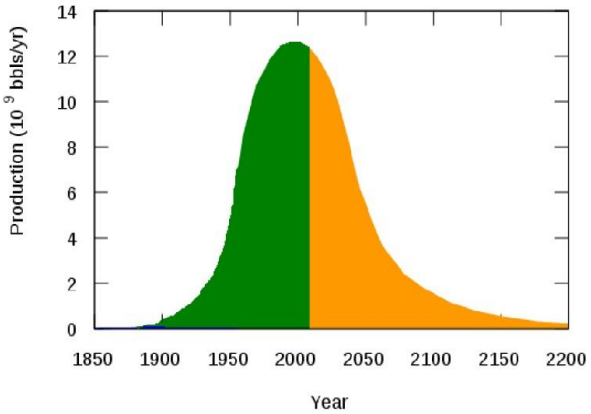

FIGURE 1. The first wake up by Hubbert [2]

In addition, fossil fuels have a serious bad effect on the environment and human health as they cause greenhouse gases emission, acid rain formation and global warming. Subsequently, the world will face a large energy depletion crisis so even it is expected, the

people will fight for it and increasing global energy demand. Solution of this problem is to make use of renewable sources of energy. In this context, it is very important to do much more research effort in this field of wind energy [3-8]. The studies dealing with the vertical axis wind turbine for development of low cost reliable wind energy converters needed for the off-grid power generation at low wind speed are still not reasonable compared to those dealing with the horizontal axis wind turbine. Much more attentiveness was paid to the small-scale wind turbines for distributed energy systems [6-12]. The Savonius-style wind turbine (SSWT) is considered promising for such conditions, comparing to horizontal axis wind turbine it has lower efficiency. Savonius designed this type of wind turbine in 1920 [13]. The maximum efficiency of this type reported by Savonius was 31%, but this result was not agreed by subsequent investigators [14-16]. Sandia Laboratories reported 24.4% as the maximum conversion efficiency of the conventional SSWT [17]. SSWT's have a number of advantages compared to other wind turbine-targeting small-scale energy conversion, as they are independent on wind direction and there is no need to yaw mechanism. Design simplicity, ease fabrication, ease of installation in small limited spaces like rooftops, and operating at low wind speed are of advantages of SSWT's [15, 16, 18-23]. The SSWT's will be a charming source of power generation if a higher efficiency can be provided.

In the last decades, a group of researchers worked to improve the efficiency and starting performance of SSWTs by using augmentation techniques, and with multi-staging in addition to the parametric analysis [16, 23]. The conventional semi-circular blades are the main shape design that most of these studies are revolved around it. A few researchers carried out the performance analysis with twisted and helical blades, despite the efficacy in performance, more complications and expenses for designs have been reported. Deflectors, guide vanes, nozzles or curtains placed upstream to turbine blades also are used to improve the performance coefficients and static torque characteristics. However, these lead to the turbine system more direction dependent and complex [16]. More complexity in design modification should probably not be encouraging, as one of the major benefits of SSWT is its design simplicity. Independency to wind direction and low cost, are also considered factors to have optimum design. In the current study, the turbine performance measured in a low speed wind tunnel under open type test section experiment [24] is compared and verified through CFD analysis.

2. METHODOLOGY

2.1. Design and Operating Parameters

The ratio between the wind turbine tip speed and free stream wind velocity is called tip speed ratio λ, and is defined by the equation (1) [25].

$$\lambda = \frac{\omega R}{V_w} \quad (1)$$

Where ω is the rotational speed of the wind turbine, R is the tip radius of the wind turbine, and the V_w is the upstream wind speed.

The efficiency of the wind turbine can be measured in terms of power coefficient C_p, and torque coefficient C_t, at different values of Reynolds number R_e, which is related to wind speed, the wind turbine diameter, and is defined as follows.

$$R_e = \frac{V_w D}{\nu} \quad (2)$$

Where ν is the kinematic viscosity of the air.

The power coefficient C_p, is defined as the ratio between the useful power output of the wind turbine, and the available power in the upstream wind [25], and is written as:

$$C_p = \frac{T\omega}{\frac{1}{2}\rho V_w^3 A} \quad (3)$$

$$C_t = \frac{T}{\frac{1}{2}\rho V_w^2 A R} \quad (4)$$

Using equations (1, 3, and 4), the relationship between the wind turbine's power, and torque coefficients can be defined as shown in equation (5).

$$C_p = \lambda C_t \quad (5)$$

2.2. Geometry Construction and Grid Generation

In this study, (ANSYS, Inc. Release 16.0) software [26] has been used to construct the geometry and generate the grid. Where the geometry in this case study is constructed, and then generates the two-dimensional fine triangles cells more than 117,000 cells, with sufficient quality of maximum orthogonal skewness equal 0.54.

The results of wind tunnel experiment [24] will be compared to the results of the CFD model presented by the current paper. The selected wind turbine model is shown in "Fig.2", the end plates are fixed at the top, and at the bottom of the wind turbine to improve the pressure difference between the convex and concave surfaces, the height of the turbine (H) to end plate diameter (Do = 1.1 D) ratio is maintained at 1, watching H = D_o = 230 mm, the blades of thickness 0.63 mm.

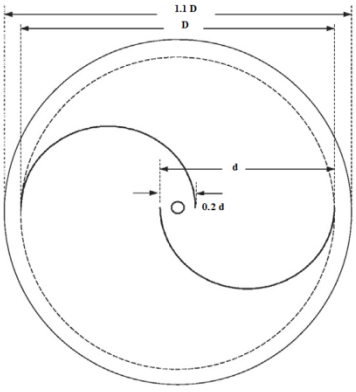

FIGURE 2. Conventional semi-circular model

2.3. Computational Domain and Boundary Conditions

In the current study, for the wind turbine, the computational domains divided into two zones as (stationary zone and rotating zone) as shown in "Fig. 3" the stationary zone is rectangular in shape, its dimensions mimic those of the test section in the wind tunnel previously described by Roy et.al. [24], with defined inlet velocity and outlet pressure boundary conditions while other sides are symmetry boundaries. The rotating zone (turbine zone) has diameter 1.2D [27].

The inlet and outlet boundary conditions of the computational domain are defined as velocity inlet and pressure outlet, respectively. The value of the inlet velocity is defined according to Renolds number (R_e), while a specified static pressure (atmospheric pressure of 101325 pa) is at outlet domain boundary. The side domain boundaries are defined as symmetric boundaries as shown in "Fig.3".

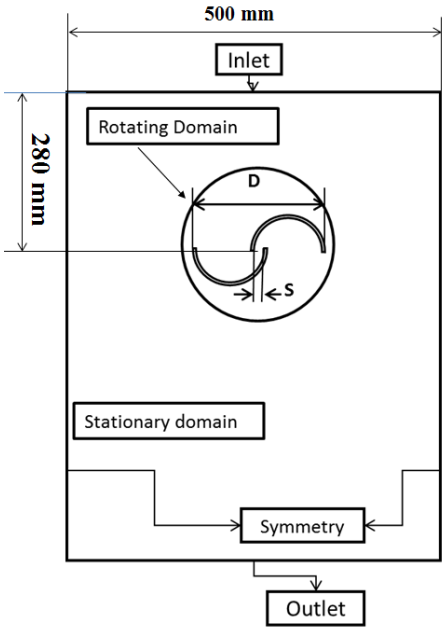

FIGURE 3. Computational domain

2.4. Computational Grid

ANSYS Meshing tool was used to descretize the calculation domain [26] into descretize control volumes (finite volumes) in order to solve the partial deferential equations numerically. One grid was created; all the cells are triangles as meshing method, the triangular edge element has the advantage of being able to model very complex geometries [28]. While creating the mesh, several parameters were taken into considerations, such as cell skewness and cell aspect ratio. Cell skewness describes how much the cell is distorted in relative to its ideal shape. If all angles of triangle cell are 60 degrees, this cell has zero skewness. Highly skewed cells are unacceptable because the equations, that being solved. In the current study, the grids were constructed with maximum skewness not exceeding 0.5 which is good [27], and the grid consists of two zones; fixed zone while the other is rotating sliding zone, as shown in "Fig 4". The entire computational domain including sliding zone was discretized using triangle control volumes.

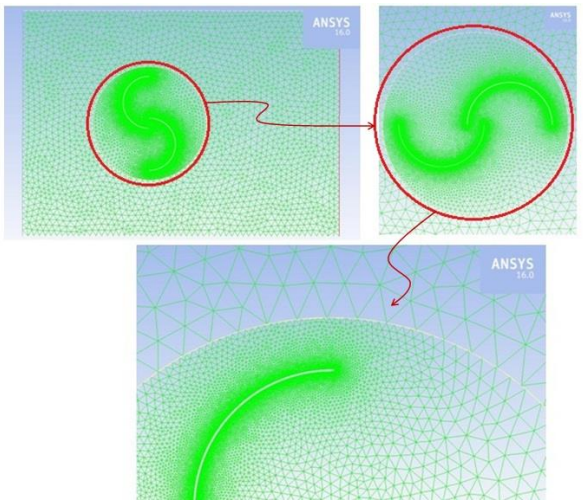

FIGURE 4. The triangle grid

2.5. Grid Independency

The discrete solution- called also, the numerical solution depends on number of control volumes within the computational domain. The calculated values are calculated at centroids of control volumes. The solution accuracy increases as the number of cells increases while the computational time will increase. Consequently, a good mesh distribution and quality is necessary to give a compromise accurate solution with less computational time. This is followed by grid independence test to obtain the least number of cells, which does not affect the examined parameter solution results. The Grid Independent Limit (GIL) is the limit where no variation in results is observed.

Torque coefficient C_t was taken as the examined parameter and grid refinements were carried out until a constant value of torque coefficient C_t was achieved. The grid density was increased by multiples of 1.1. Each case was solved while maintaining the same input parameters in ANSYS-Fluent 16 [26]. This test was performed for generated grid with triangle cell at tip-speed ratio of 0.38377 as demonstrated in table (1).

TABLE 1. Grid independence test for triangle mesh

Triangle Grid			
No. of cells	C_t	No. of cells	C_t
101860	0.3755	131891	0.3719
107611	0.3724	141716	0.3728
114669	0.3709	155887	0.3718
122535	0.3745	171475	0.3714

3. RESULTS AND DISCUSSION

In 2015, Roy and Saha [24] tested the two-bladed Savonius wind turbine in a wind tunnel and presented a schematic diagram of the experimental set up as shown in "Fig.5". In continuation to that work, the on-going study deals on verification of the previously reported results by using (ANSYS, Inc. Release 16.0) software [26]

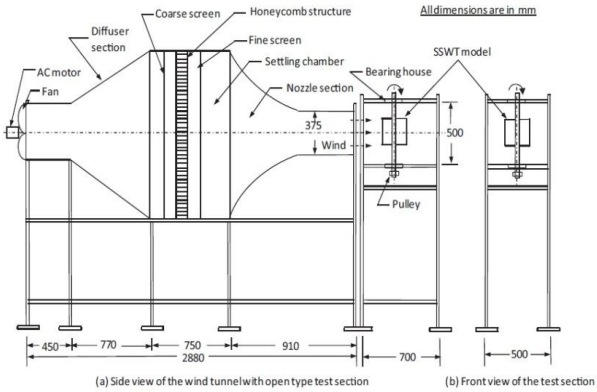

FIGURE 5. Schematic diagram of the experimental setup [24]

3.1 Numerical Flow Simulation

When the flow is steady, the accurate numerical solutions could be obtained after many cycles. The average torque coefficient was calculated at each cycle. "Fig. 6" shows average torque coefficient variation with eleven cycles at tip speed ratio 0.38 with input wind speed 6 m/s, and time step equal 0.0007924587 sec for one degree as a sample of results.

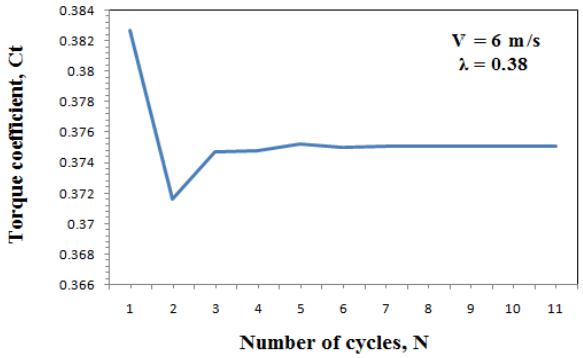

FIGURE 6. Variation of torque coefficient with number of cycles

The edges of wind turbine rotor buckets are marked as listed in table (2) in order to facilitate the tracking of x-y plotting of different variables.

TABLE 2. Names of wind turbine rotor buckets edges

Edge type	Bucket number	Edge name
Concave	A	Blade 1
Convex	A	Blade 2
Concave	B	Blade 4
Convex	B	Blade 3

3.2. Analysis of Results

In order to study the behaviour of the Savonius wind turbine, qualitative analysis of pressure and velocity contours was applied. More over a pressure coefficient is plotted on the turbine blades at different angles of rotation to show the drag forces contribution to torque producing mechanism are shown in "Fig. 7".The three depicted different turbine angels are as follows:

i- $\theta = 0^{\circ}$: A stagnation point at the middle of the returning bucket (bucket B) was formed due to the high relative velocity of the resisting flow that stagnated at that point. The positive torque has been produced by the advanced bucket (bucket A) but with small value compared to the resisting torque produced by the returning bucket leading to net negative torque.

ii- $\theta = 16^{\circ}$: The resisting flow faced by returning bucket will start to decrease when the wind turbine start to rotate, and returning bucket advances in air as blockage projected area start to decrease. The stagnation point starts to move outwards on the bucket B when the bucket advances in air until it disappears meanwhile, another stagnation point is developing on bucket A that became now the returning bucket.

iii- $\theta = 110^{\circ}$: Zone of low pressure is formed behind the advancing bucket A, and increasing gradually as the angle of rotation is increasing.

i **$\theta = 0^{\circ}$**

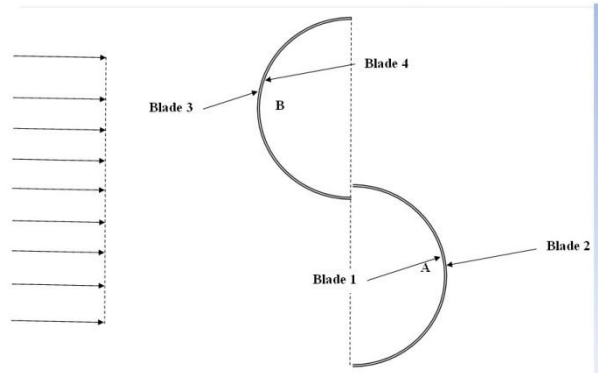

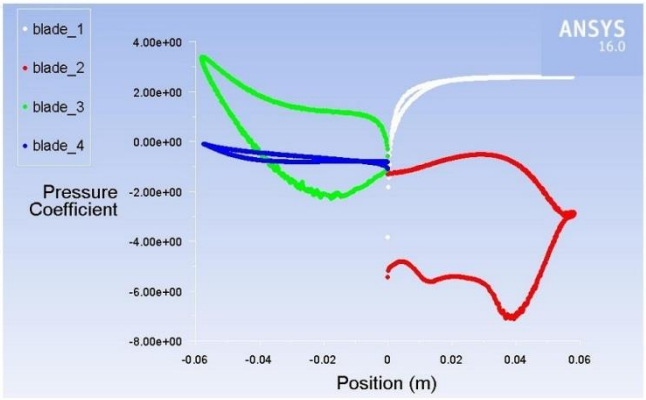

a- Pressure coefficient plot

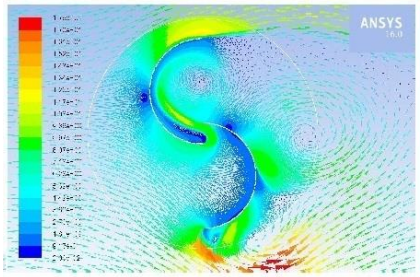

b- Velocity vectors

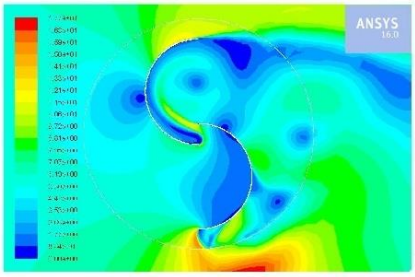

c- Velocity contours

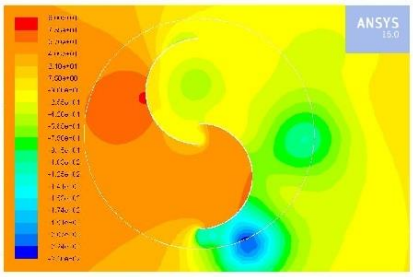

d- Static pressure contours

ii **ɵ = 16**

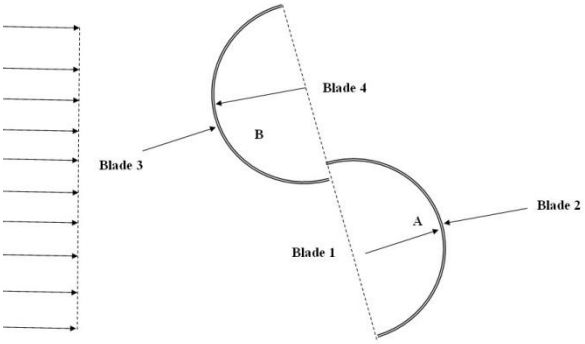

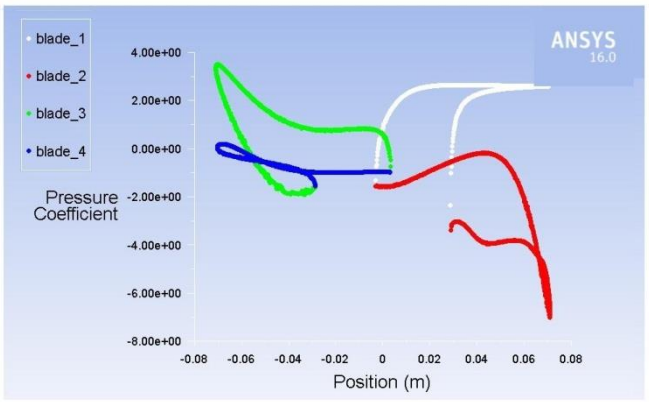

a- Pressure coefficient plot

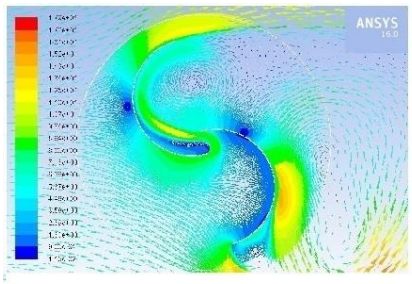

b- Velocity vectors

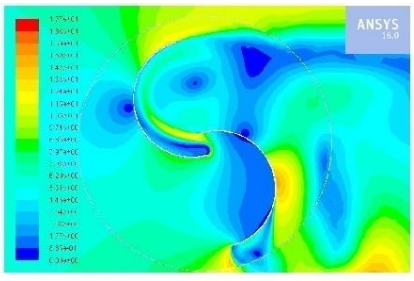

c- Velocity contours

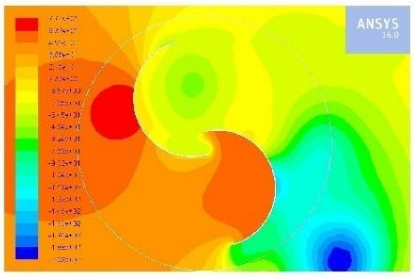

d-Static pressure contours

iii **ɵ = 110˚**

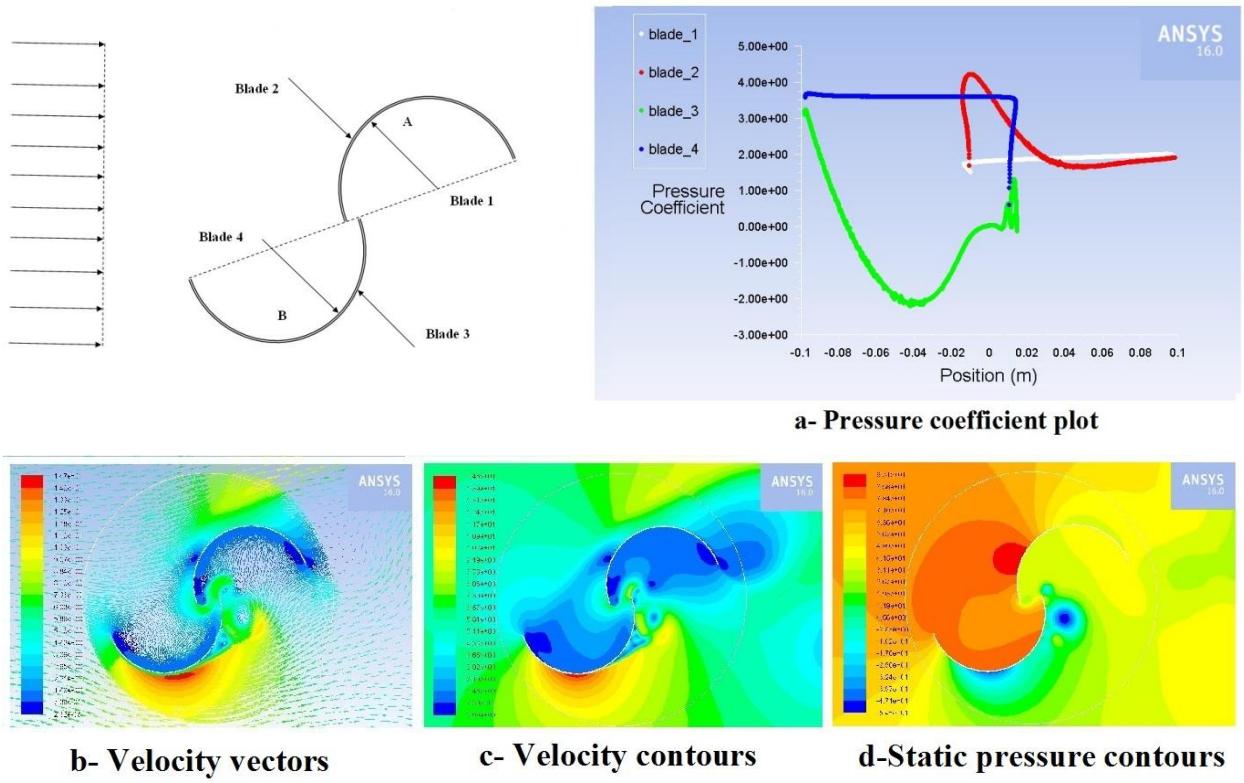

FIGURE 7. Pressure coefficient plot, velocity vectors, velocity contours, and static pressure contours at: (i) ɵ = 0°, (ii) ɵ = 16°, and ɵ = 110°

The validation of torque coefficient C_t results obtained by Roy and Saha [24] with respect to the results obtained by CFD at tip speed ratio λ ranges from 0.67 to 0.74 is plotted as shown in "Fig. 8". Absolute error was also depicted at the same values of λ. While "Fig. 9" depicts the validation of torque coefficient C_t results obtained by Irabu and Roy [29] with respect to those obtained by Roy and Saha [24] at the same range of λ (0.67 to 0.74). Absolute error was also depicted at the same values of λ. Obviously, the two figures showed that the absolute error increases as the value of λ increases.

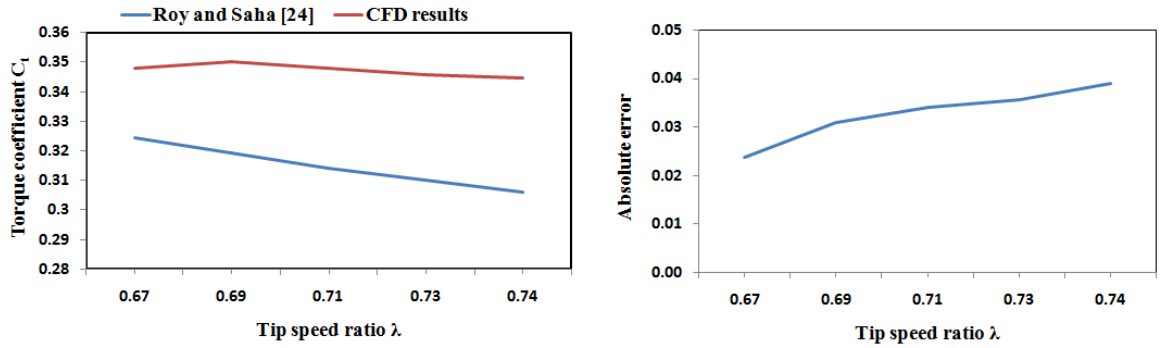

(a) (b)

FIGURE 8. (a) Validation of torque coefficient C_t by Roy and Saha [24] with CFD results versus tip speed ratio λ; (b) Absolute error versus tip speed ratio λ.

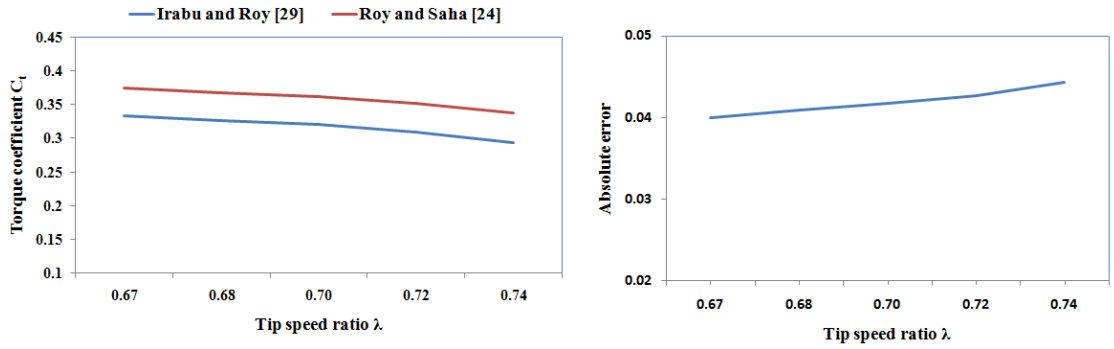

(a) **(b)**

FIGURE 9. (a) Validation of torque coefficient C_t by Irabu and Roy [29] with Roy and Saha [24] results versus tip speed ratio λ; (b) Absolute error versus tip speed ratio λ.

4. CONCLUSION

In view of the importance of improving the efficiency of two-bladed, Savonius-style wind turbine (SSWT) specifically meant for small-scale wind energy conversion, the present work presents the results of computational fluid dynamic (CFD) work and compare them with those of wind tunnel experiments in the previous studies. Studying the effect of wind speed on the performance of (SSWT) with conventional semi-circular two blades is very important in order to enhance the performance of two-bladed Savonius-style wind turbine (SSWT). The computational fluid dynamics (CFD) by using (ANSYS, Inc. Release 16.0) [26] was able to accurately predict the performance of (SSWT) with conventional semi-circular two blades. The results showed that the absolute error is directly proportional to the tip speed ratio λ, this is in accordance with the results presented in the previous studies. The order of increasing in the absolute error ~ 0.01. Further studies by using Adjoint Solver to modify the geometry of the turbine blades in order to maximize the efficiency are still recommended.

5. REFERENCES

[1] S. Shafieeand E. Topal, Journal of Energy Policy **37**, 181-189 (2009).

[2] T. Al-Shemmeri, Wind Turbines, T. Al-Shemmeri & Ventus Publishing Aps, 2010

[3] S. Rolland, W.Newton,A. J. Williams, T.N. Croft, D.T.Gethin, and M. Cross, Appl. Energy**111**, 1195-1203 (2013).

[4] W. T. Chong, S. C. Poh, A.Fazlizan, S. Y. Yip, C. K. Chang, and W. P. Hew Appl. Energy**112**, 568-575 (2013).

[5] S. Obara, Y. Morizane, and J. Morel, Appl. Energy**111**, 358-373 (2013).

[6] D. Saeidi, A.Sedaghat, P.Alamdari, and A. A.Alemrajabi, Appl. Energy**101**, 765-775 (2013).

[7] L. A. Danao, O.Eboibi, and R. Howell, Appl. Energy**107**,403-411 (2013).

[8] T. Morbiato, C.Borri, and R. Vitaliani, Appl. Energy**116**, 111-124 (2014).

[9] L. A. Danao, J. Edwards, O. Eboibi, and R. Howell, Appl. Energy **116**,111-124 (2014).

[10] S. A. Rolland, M. Thatcher, W. Newton, A. J. Williams, T. N. Croft, D. T. Gethin, et.al.,Appl. Energy**111**,1183-1194 (2013).

[11] W. T. Chong, A.Fazlizan, S. C.Poh, K. C. Pan, W. P. Hew, and F. B. Hsiao, Appl. Energy**112**,601-609 (2013).

[12] F. Balduzzi, A. Bianchini, E. A. Carnevale, L. Ferrari, and S. Magnani, Appl. Energy**97**, 921-909 (2012).

[13] P. D. Fleming, S. D. Probert, and D. Tanton, Appl. Energy**19**, 97-110 (1985).

[14] M. A. Kamoji, S. B. Kedare, and S. V. Prabhu, Appl. Energy**86**, 1061-1073 (2009).

[15] S. Roy and U. K. Saha, Renew Sustain Energy Rev**24**, 73-83 (2013).

[16] S. Roy and U. K. Saha,ProcIMechE Part A: J.Power Energy,**227**, 528-542 (2013).

[17] A. H. Benesh, Wind turbine with Savonius-type rotor. US Patent; 1996, No.5494407.

[18] K. Golecha, T. I.Eldho, and S. V.Prabhu,Appl. Energy, **88**, 3207-3217 (2011).

[19] J. P. Abraham, B. D.Plourde, G. S. Mowry, W. J. Minkowycz, and E. M. Sparrow, J Renew Sustain Energy**4**, 1-21(2012).

[20] B. D. Plourde, J. P. Abraham, G. S. Mowry, and W. J. Minkowycz, Sens Transducers **61**,13-53 (2011).

[21] B. D. Plourde, J. P. Abraham, G. S. Mowry, and W. J. Minkowycz,Wind Eng. **36**,443-454 (2012).

[22] J. P. Abraham, B. D. Plourde, G. S. Mowry, E. M. Sparrow, and W. J. Minkowycz,J Renew Sustain Energy **3(033109)**, 1-13 (2011).

[23] J. V. Akwa, H. A. Vielmo, and A. P. Petry, Renew Sustain Energy Rev **16**, 3054-3064 (2012).

[24] R. Sukanta, K. S. Ujjwal, Appl. Energy **137**, 117-125 (2015).

[25] B. M. Shaughnessy, and S. D. Probert, Appl. Energy **43**, 239-249 (1992).

[26] ANSYS, Inc. Release 16.0, Southpointe 2600 ANSYS Drive Canonsburg, PA, 15317 (2015). ansysinfo@ansys.com, http://www.ansys.com

[27] F. Balduzzi, A. Bianchini, R. Maleci, G. Ferrara and L. Ferrari, Renewable Energy **85**, 419-435 (2016).

[28] J. Y. Wu, and R. Lee, IEEE Transaction on Antennas and propagation **45**, 1431-1437 (1979).